AIP Advances

Interface formation and Schottky barrier height for Y, Nb, Au, and Pt on Ge as determined by hard x-ray photoelectron spectroscopy

Cite as: AIP Advances **13**, 015305 (2023); https://doi.org/10.1063/5.0101688
Submitted: 30 August 2022 • Accepted: 24 December 2022 • Published Online: 06 January 2023

Abdul K. Rumaiz, Conan Weiland, Ian Harding, et al.

Interface formation and Schottky barrier height for Y, Nb, Au, and Pt on Ge as determined by hard x-ray photoelectron spectroscopy

Cite as: AIP Advances 13, 015305 (2023); doi: 10.1063/5.0101688
Submitted: 30 August 2022 • Accepted: 24 December 2022 •
Published Online: 6 January 2023

Abdul K. Rumaiz,[1,a)] Conan Weiland,[2] Ian Harding,[3] Neha S. Nooman,[4] Thomas Krings,[5] Ethan L. Hull,[6] Gabriele Giacomini,[3] Wei Chen,[3] Eric Cockayne,[2] D. Peter Siddons,[1] and Joseph C. Woicik[2]

AFFILIATIONS

[1] National Synchrotron Light Source II, Brookhaven National Laboratory, Upton, New York 11973, USA
[2] National Institute of Standards and Technology, Gaithersburg, Maryland 20899, USA
[3] Instrumentation Division, Brookhaven National Laboratory, Upton, New York 11973, USA
[4] Department of Electrical Engineering, Stony Brook University, Stony Book, New York 11974, USA
[5] Forshungzentrum, Juelich, GmbH, Juelich 52428, Germany
[6] PHDs Co., Knoxville, Tennessee 37921, USA

[a)] **Author to whom correspondence should be addressed:** rumaiz@bnl.gov

ABSTRACT

Development of a robust, thin, hole-blocking (n+) contact on high purity germanium (HPGe) has been the main challenge in the development of Ge-based radiation sensors. Yttrium has been reported to be a viable hole-blocking contact on HPGe, and detectors with low leakage have been fabricated. Niobium has also been considered as a potential hole-blocking contact due to its low work function. Here, we investigate interface chemistry and the Schottky barrier height of Y and Nb, as well as electron-blocking contacts Au and Pt, on Ge(100) surfaces using hard x-ray photoelectron spectroscopy. We find a barrier height of 1.05 ± 0.10 eV for Y/HPGe, confirming the formation of a hole-blocking barrier. For Nb/HPGe, the barrier height of 0.13 ± 0.10 eV demonstrates that the interface is not hole-blocking. The Schottky barrier of Au and Pt was found to be 0.45 ± 0.10 and 0.51 ± 0.10 eV, respectively.

I. INTRODUCTION

Semiconductor heterojunctions are the backbone of most modern electronic devices, and understanding the energy band alignment of the heterojunctions is critical in the design and performance of such devices.[1,2] Selective control of charge transport across a heterojunction is achieved by means of band discontinuities across the heterojunctions. For example, a large conduction band offset and a small valence band offset block the transport of electrons while allowing the transport of holes. Conversely, a large valence band offset and a small conduction band offset act as a hole-blocking contact. A low dark/leakage current is crucial to minimize noise and to achieve the high applied voltage needed for full depletion of the detector. Thus, effective semiconductor radiation detectors require both robust electron-blocking and hole-blocking contacts to provide good charge collection efficiency while maintaining low leakage current.[3–5]

High purity Ge (HPGe)/detector-grade Ge is often used in devices for detection of high-energy x rays and gamma rays. While the availability of high-quality detector-grade materials has led to the development of efficient detectors with reasonable depletion voltages and excellent charge collection efficiencies, the full potential of Ge-based radiation sensors has not been realized due to the lack of reliable, thin, hole-blocking (n+) contacts. For example, complicated device geometries, such as the drift sensor and charge-coupled devices (CCDs), which are possible in Si-based devices, are not yet

feasible with Ge because hole-blocking layers cannot be precisely made separate from electron-blocking (p+) contacts on the same side of the device.[10] Thin electron-blocking contacts can be easily achieved either by depositing metals, such as Au, Ni, or Cr, on Ge or by forming a thin B-doped p+ contact,[6–9] but hole-blocking contacts are traditionally achieved by a thick Li-diffused layer in Ge, and the diffused layer tends to be 100's of μm thick, rendering any lithography or segmentation challenging.

The development of a reliable hole-blocking contact for Ge is an ongoing effort. An early alternative to a Li-based hole-blocking contact was amorphous semiconductor contacts, which were promising because the band tailing in amorphous semiconductors above and below the valence band maximum and conduction band minimum, respectively, implies that the same layer could be used for both hole and electron-blocking contacts. While detectors fabricated with such contacts are now commercially available,[11] they suffer from high leakage and instabilities under a heavy radiation environment. Recently, Y has been shown to work as a hole-blocking contact on HPGe,[12,13] and numerous fully depleted Ge detectors with sputtered Y contacts were fabricated with low leakage current and good charge collection efficiency. While a simplistic analysis based on the Y work function does provide evidence of hole-blocking band alignment, more detailed and precise measurements of the alignment have yet to be performed. Here, we use hard x-ray photoelectron spectroscopy (HAXPES) measurements together with density functional theory (DFT) calculations of the density of states to measure the Schottky barrier height of Y on Ge precisely. We also measure the Schottky barrier height for Nb on Ge because Nb is another potential hole-blocking contact material due to its low work function. Well-known electron-blocking layers, Au and Pt, were also measured for comparison. The longer inelastic mean free paths in HAXPES compared to conventional photoelectron spectroscopy allow the direct measurement of buried interfaces and thus a precise measurement of the Schottky barrier height.

II. EXPERIMENTAL DETAILS

Prior to metal deposition, HPGe wafers were dipped in dilute H_2O_2 followed by thorough rinsing in de-ionized water to remove the native oxide. For metal deposition, the base pressure of the chamber was 10^{-5} Pa, which is the typical environment for detector device fabrication (SOURCE). For heterojunction samples, a layer of metal of 2–3 nm thickness was sputtered (with exception to Au, which was evaporated); in the cases of Y and Nb, each was presputtered prior to deposition to further lower the partial pressure of O in the chamber. For the reference sample required for the Schottky barrier measurement, a thick film (greater than 100 nm) was deposited under identical conditions. Y reference was collected with a commercial high purity Y target. All depositions were performed in the same chamber.

DFT calculations to determine the Ge electronic structure and partial density of states were performed using the Vienna *Ab initio* Simulation Package (VASP) software program.[14,15] The Perdew-Burke-Ernzerhof adapted for solids (PBEsol) generalized gradient approximation (GGA) was used for the exchange-correlation functional.[16] Projector augmented wave pseudopotentials[17] were used. The calculations were performed with a plane-wave cutoff energy of 500 eV and a Γ-centered 24 × 24 × 24 k-point grid for a cubic eight-atom Ge cell. Full density functional theory and experimental data are available on the NIST Public Data Repository.[18]

HAXPES measurements were performed at the NIST SST-2 beamline of the National Synchrotron Light Source II, Brookhaven National Laboratory. HAXPES data were collected using the Si(111) reflection from a double-crystal monochromator and a hemispherical electron analyzer that had its acceptance cone oriented parallel to the x-ray electric polarization vector of the incident beam and perpendicular to the beam propagation direction. All the data were collected with a photon energy of 2000 eV and a pass energy of 20 eV. The takeoff angle during measurement was set at 80°. Details of the

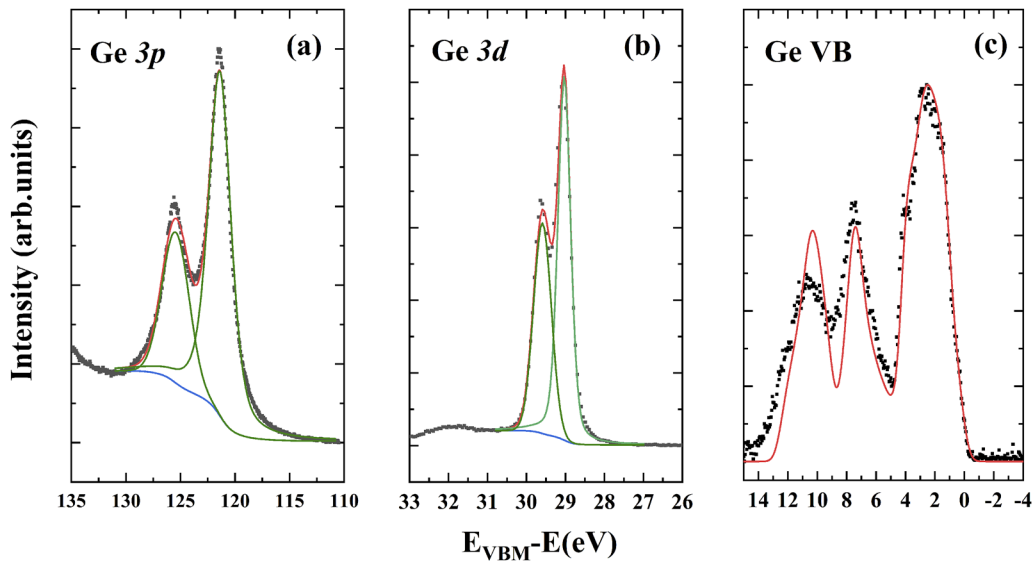

FIG. 1. HAXPES spectra for HPGe reference. (a) High-resolution Ge 3p spectra showing curve fitting. (b) High-resolution Ge 3d spectra and fitting. (c) Comparison of Ge valence bands with cross section weighted theoretical DOS. The black dots are experimental VB, and the red line is the cross section weighted DOS.

beamlines, vacuum systems, and experimental procedures have been presented previously.[19]

To evaluate any metal for applicability as a hole-blocking contact on a semiconductor, it is imperative to understand the band alignment precisely. Band alignment for idealized heterojunctions, in particular at metal–semiconductor interfaces, can be roughly estimated by difference of work function of the two materials via Anderson's rule.[20] However, this estimation does not account for band-discontinuity contributions due to interface dipoles, and other effects, for example, those caused by diffusion at the heterojunction.[21] These contributions account neither for chemistry nor for the interface structure and can alter the transport properties significantly. Thus, a useful measurement of band lineup for the purposes of determining the effectiveness of the hole-blocking layer must have a high level of accuracy. Photoelectron spectroscopy is one such measurement technique that can measure the position of the valence band with tremendous accuracy, and, furthermore, HAXPES offers the unique advantage of the ability to probe buried layers. Thus, together with the increased information depth of HAXPES, we can simplify the measurement by directly probing the semiconductor–metal interface in an actual heterojunction. Moreover, HAXPES is also sensitive to interface dipoles since the subtle shift due to interface dipoles can be observed as a shift of the core-level energy.

We use Kraut's method[22] for calculating the band offsets; this method is based on the fact that the energy separation between the valence band maximum (VBM) and the core levels of the substrate remains unchanged after the metal deposition. Briefly, the valence band offset is determined by referencing the core-level energies in the heterojunction to that of the respective standalone materials or sufficiently thick films. For the case of metal on Ge, the valence offset ΔE_V is given by

$$\Delta E_V = (E_{\mathrm{Ge}3d} - E_{\mathrm{GeVB}})_{Semiconductor} - (E_{CL} - E_F)_{Metal} - (E_{\mathrm{Ge}3d} - E_{CL})_{Heterojunction}, \quad (1)$$

where $E_{\mathrm{Ge}3d}$ and E_{GeVB} are the peak position of the Ge 3*d* core line and the VBM, respectively, and E_{CL} and E_F are the peak position of the metal core line and Fermi level, respectively. The values of E_{CL} and E_F can be obtained with appropriate curve fitting; the highest uncertainty lies in the precise determination of the VBM of the semiconductor owing to the inherently non-symmetric line shapes. For precise VBM determination, we compare the Ge valence band to the sum of the individual orbital angular momentum resolved partial density of states weighted by the photoionization cross sections.[23,24] The resulting curve is further convolved with a Gaussian function to account for experimental broadening.

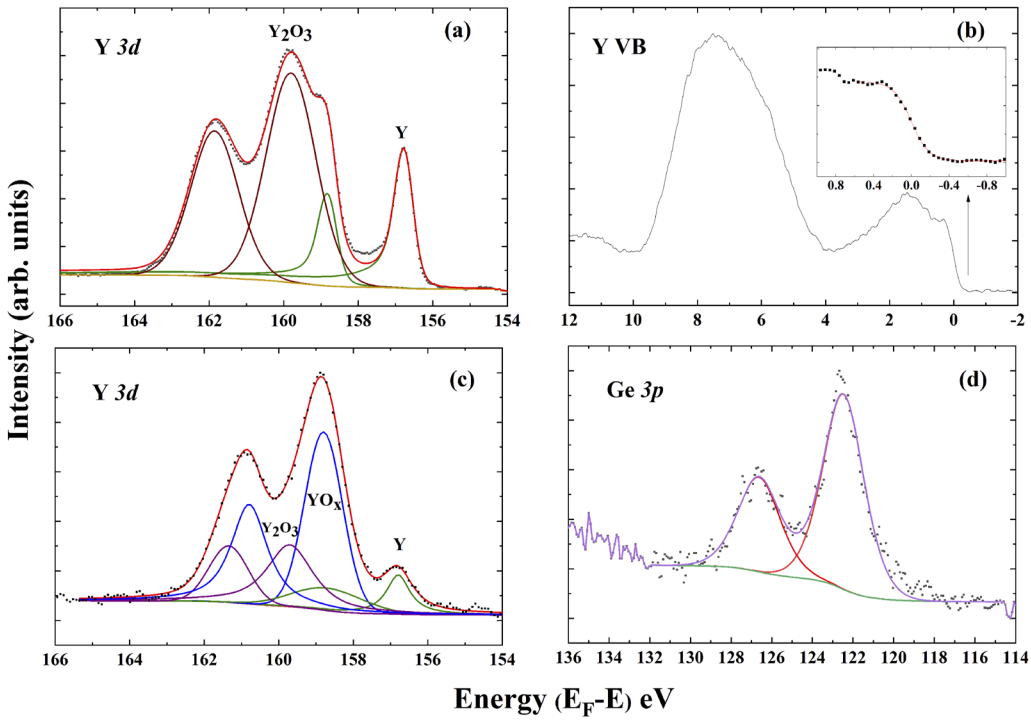

FIG. 2. (a) HAXPES spectrum of the Y $3d_{5/2}$ and $3d_{3/2}$ core levels, measured on the sputtered reference film and fitted with two spin–orbit doublets corresponding to Y^0 and YO_x. (b) Valence band spectra of the Y reference film; the inset shows the fit of the Fermi level to a Fermi function. The reference spectra were collected at $h\nu$ = 6000 eV on a Y metal target. (c) Y 3*d* core line from the Y/HPGe heterojunction fitted with three spin–orbit doublets corresponding to Y^0 and two sub-oxide states. (d) Ge 3*p* from the Y/HPGe heterojunction showing a single spin–orbit doublet from Ge^0. The spectra have been referenced to the Y Fermi level as indicated.

III. RESULTS AND DISCUSSION

Figures 1(a) and 1(b) show the Ge 3*p* and Ge 3*d* core lines, respectively, collected at photon energy $h\nu$ = 2000 eV. Both spectra show the expected doublet due to the spin–orbit splitting. All core-level data were fitted with Voigt functions keeping the branching ratio fixed to theoretical values for each core. For Ge 3*d*, the Ge^{4+} oxidation state is reported to be chemically shifted ~3 eV from Ge^0;[25] only a very weak feature at 32 eV binding energy is observed, revealing a clean Ge signal. The background-subtracted valence band measurement and comparison with cross section weighted theoretical DOS are shown in Fig. 1(c). The VBM was set to 0, and all core lines in Fig. 1 are referenced with respect to the Ge VBM.

Figure 2(a) shows the Y $3d_{5/2}$ and Y $3d_{3/2}$ core level of the reference Y metal target (dots) along with peak fitting. To increase the relative intensity of the metallic Y component, the data were collected at a photon energy of 6000 eV. The spectrum shows oxidized Y, with a low binding energy peak indicative of the metallic Y^0 state. The peak separation between the Y^0 and the higher oxidation state is ~3.0 eV; this is close to the reported chemical shift for Y_2O_3 (~2.7 eV).[26] The valence band shows a dominant O 2*p*, and a strong Y metal Fermi level. The inset of Fig. 2(b) shows the fit with a Fermi function. Figures 2(c) and 2(d) show the Y 3*d* and Ge 3*p* core lines from the heterojunctions, respectively. The Ge 3*p* core line was used for band alignment calculations due to overlap of the Y 4*p* core line with Ge 3*d*. Y 3*d* has been fitted with multiple Voigt peaks corresponding to Y^0 and oxide peaks corresponding to YO_x and Y_2O_3.[27] The heterojunction sample spectra also show a relative increase in the oxide intensity compared to the Y metal reference peaks. The increased presence of Y oxides in the heterojunction samples can be attributed to gettering of O from native GeO at the interface.[28] Nonetheless, the Y^0 oxidation state can be identified clearly from the 3*d* peak. Analysis of the Ge 3*p* core line shows a clear Ge^0 oxidation state with no evidence of high oxidation components.

Figure 3(a) shows spin–orbit splits of the Nb 3*d* core line of the reference sputtered Nb films. The spectra could be best fit with six doublet peaks. The peaks correspond to the Nb metal (fit with Doniach–Sunjic line shapes[29]) and four oxides of Nb (fit with Voigt line shapes). The oxides correspond to NbO_x (x < 1), NbO, NbO_2, and Nb_2O_5 based upon previously reported peak fitting;[28] however, only the metallic Nb^0 component is used for the analysis here.[30] Figure 3(b) shows the valence band spectrum of reference Nb. The top of the VB shows the dominant Nb 4*p* line, which was fit with a Fermi function to determine E_F. As expected, the VB has a strong O 2*p* contribution due to oxidation; however, there is still significant signal from the metallic Nb allowing for measurement of E_F. Figures 3(c) and 3(d) show the core lines of Nb and Ge from the heterojunctions. As above, we used Ge 3*p* as the reference due to overlap of the Nb 4*p* core line with the Ge 3*d* core line. Similar to the case of Y, the increased presence of Nb oxides in the heterojunction samples can be attributed to gettering of O from any native GeO at

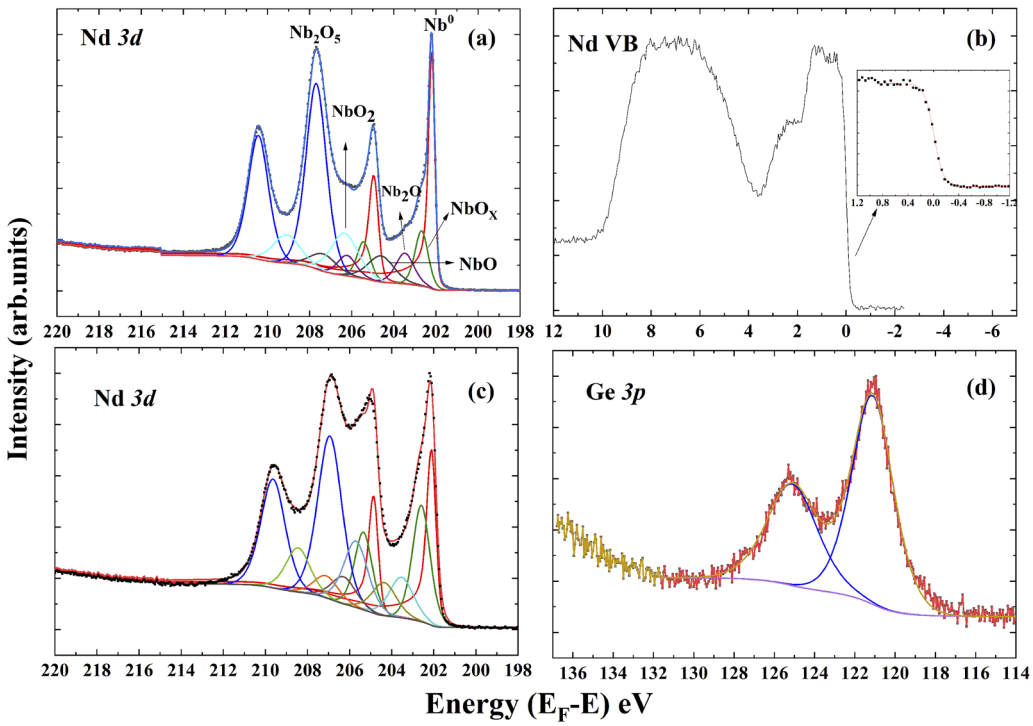

FIG. 3. (a) HAXPES spectrum of the Nb $3d_{5/2}$ and $3d_{3/2}$ core levels, measured on the sputtered reference film and fitted with five oxide components. Metallic components are fit with Doniach–Sunjic line shapes, while the oxide components are fit with Voigt shapes. (b) Valence band spectra of Nb. The inset shows the fitting to a Fermi function. (c) HAXPES measurement of Nb 3*d* from the Nb/Ge heterojunction, with fitting as in Fig. 3(a). (d) Ge 3*p* core line from the Nb/Ge heterojunction fit with a single spin–orbit doublet. The black dots are experimental VB, and the red line is the cross section weighted DOS.

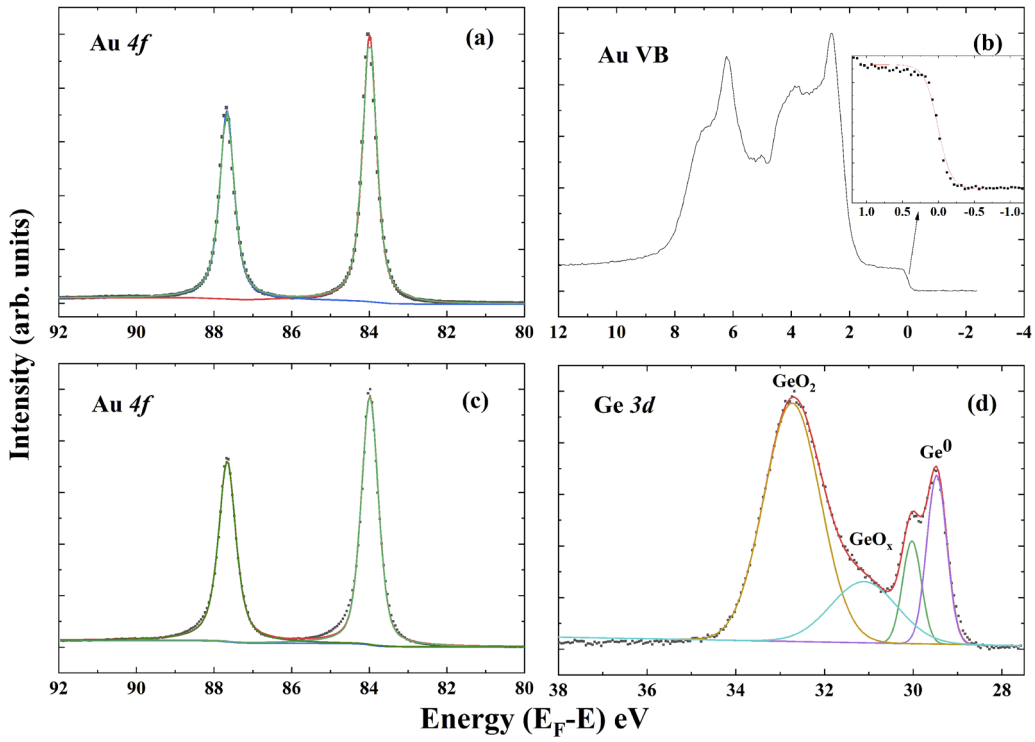

FIG. 4. (a) High-resolution Au 4*f* spectra from an Au reference film fitted with a single spin–orbit doublet. (b) Valence band of the Au reference. The inset shows the Fermi Level fit to a Fermi function. (c) Au 4*f* from the Au/Ge heterojunction, fitted with a single spin–orbit doublet. (d) Ge 3*d* core line from the Au/Ge heterojunction, fit with a spin–orbit doublet for Ge^0, and singlets for two oxide binding states. The black dots are experimental VB, and the red line is the cross section weighted DOS.

the interface.[28] As in the reference Nb film, the heterojunction Nb 3*d* [Fig. 3(c)] has been fit with multiple peaks corresponding to the Nb^0 oxidation state and various oxides of the metal. The spectra also show a clear increase in the oxide intensity compared to the metal reference peaks. Nevertheless, the Nb^0 oxidation state can be clearly identified.

Figures 4(a) and 4(b) show the high-resolution Au 4*f* core line and valence band of the reference Au film, respectively. Au 4*f* shows the characteristic spin–orbit doublet with separation of ~3.75 eV. The VB for the Au reference film shows the characteristic Fermi foot at the VBM. The inset shows the fitting of the top of the valence band to a Fermi function. Figures 4(c) and 4(d) show the core lines of Au on Ge. The Au/Ge interface shows the characteristics of the Au 4*f* core line with a single binding state. However, the Ge 3*d* [Fig. 4(d)] is best fit with four peaks: two corresponding to the spin–orbit doublet of the Ge 0+ oxidation state, and two broad oxide peaks corresponding to GeO_x and GeO_2.[31] Due to the oxide formation in the Ge interface, we choose 3*d* as the reference for band alignment measurement since the Ge^0 oxidation state in Ge is well resolved in the 3*d* core line compared with the 3*p* spectra.

Figures 5(a) and 5(b) show the high-resolution Pt 4*f* and valence band of the reference Pt film, respectively. The Pt 4*f* spectra show a long high-energy tail and are best fit with a Doniach–Sunjic (DS) line shape.[29] In the Pt VB, the incomplete filling of the 5*d* level in Pt leads to an overlap of the 6*s* level at the VBM. This results in the absence of the well-separated 6*s* as in the case of Au, making fitting of the VBM to a Fermi function complicated. As a result, we used the inflection point of the edge as the position of E_F in Pt. Figure 5(c) shows the core lines of Pt from the Pt/HPGe heterojunction. The Pt/Ge interface shows a clean Pt 4*f* core line fit with a DS doublet showing one apparent binding state. Ge 3*d* on the other hand shows a more complicated line shape. Apart from the usual lower binding energy doublet corresponding to the Ge^0 oxidation state, we see several additional peaks. The peak 0.6 eV from the elemental Ge is attributed to the interfacial reaction of Pt on Ge leading to the formation of Pt-germanide (Ge_2Pt).[32] The broad peak about 3 eV from the elemental peak corresponds to the two oxides of Ge as labeled in Fig. 5(d).

It is well known that during the fabrication of typical devices involving a metal–semiconductor interface, there is generally a thin native oxide present on the surface of the semiconductor. From the Nb and Y 3*d* core-level spectra of the heterojunction sample [Figs. 2(c) and 3(c)], we see an increase in the oxide peak. Combined with the absence of higher oxidation components of Ge 3*p*, we can conclude that Nb and Y chemically react via gettering to eliminate the native oxide from Ge to form an interface region consisting of non-insulating metal and metal oxide. However, for the inert metals Au and Pt, we do see the effect of oxygen gettering at the interface. The interface oxide thickness can be estimated from the Ge 3*d* oxide to metal peak using the following equation:[33]

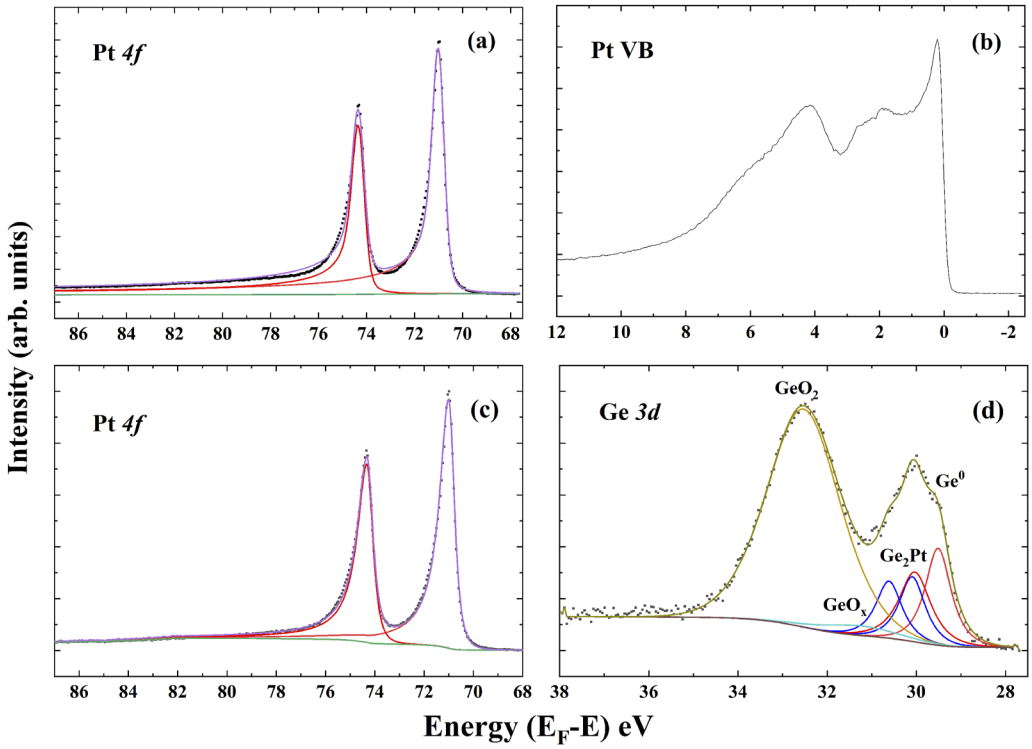

FIG. 5. (a) High-resolution Pt 4*f* core line fit with Doniach–Sunjic line shapes. (b) Valence band spectra of Pt. The inflection point was set as the Fermi level. (c) Pt 4*f* from the Pt/Ge heterojunction. (d) Ge 3*d* core line from the Pt/Ge heterojunction. The black dots are experimental VB, and the red line is the cross section weighted DOS.

$$\Delta t = \lambda_o \sin\theta \ln\left[\frac{n_{\mathrm{Ge}}\lambda_{\mathrm{Ge}} I_o}{n_o \lambda_o I_{\mathrm{Ge}}} + 1\right], \quad (2)$$

where n_{Ge} and n_o are the densities of Ge and the oxide, I_o/I_{Ge} is the metal to oxide peak ratio, and θ is the takeoff angle. λ_o and λ_{Ge} are the inelastic mean free path (IMFP) of the photoelectrons in the oxide and semiconductor, respectively. In the case of the heterojunction interface, the oxide is buried inside the metal, and therefore, the IMFP must be calculated for the overlayer metal. In other words, for oxide buried in metal layers, we can set $\lambda_o = \lambda_{\mathrm{Ge}} = \lambda_{metal}$. It is now more common to use the effective attenuation length (EAL) rather than IMFP as it considers the effect of elastic scattering. EAL was calculated for Au and Pt using the simulation of electron spectra for surface analysis (SESSA)[34] code and found to be 1.84 and 1.74 nm, respectively.[15] The oxide thickness was measured to be 2.95 and 3.55 nm for Au/Ge and Pt/Ge, respectively. While detailed modeling of Schottky barrier contacts in heterojunctions assumes the presence of a native oxide,[35] photoemission-based band alignment measurements provide a clear understanding of the chemistry at the interface, which in some cases might not be simple native

TABLE I. Schottky barrier heights measured for Au, Pt, Y, and Nb on HPGe. For comparison, we have included the barrier heights calculated using Anderson's rule. Work functions of materials were obtained from Ref. 37.

Material	Energy difference	Anderson's rule (eV)	HAXPES (eV)
Reference Ge	$E_{Ge3d} - E_{GeVBM}$: 29.02 ± 0.1 eV $E_{Ge3p} - E_{GeVBM}$: 121.39 ± 0.1 eV		
Reference Y	$E_{Y3d} - E_{Fermi}$: 156.77 ± 0.1 eV		
Reference Nb	$E_{Nb3d} - E_{Fermi}$: 202.19 ± 0.1 eV		
Reference Au	$E_{Au4f} - E_{Fermi}$: 83.98 ± 0.1 eV		
Reference Pt	$E_{Pt4f} - E_{Fermi}$: 71.02 ± 0.1 eV		
Au/HPGe	$E_{Au4f} - E_{Ge3d}$: 54.51 ± 0.1 eV	0.80	0.45 ± 0.1
Pt/HPGe	$E_{Pt4f} - E_{Ge3d}$: 41.49 ± 0.1 eV	0.97	0.51 ± 0.1
Y/HPGe	$E_{Y3d} - E_{Ge3p}$: 34.28 ± 0.1 eV	1.57	1.10 ± 0.1
Nb(001)/HPGe	$E_{Nb3d} - E_{Ge3p}$: 80.93 ± 0.1 eV	0.65	0.13 ± 0.1

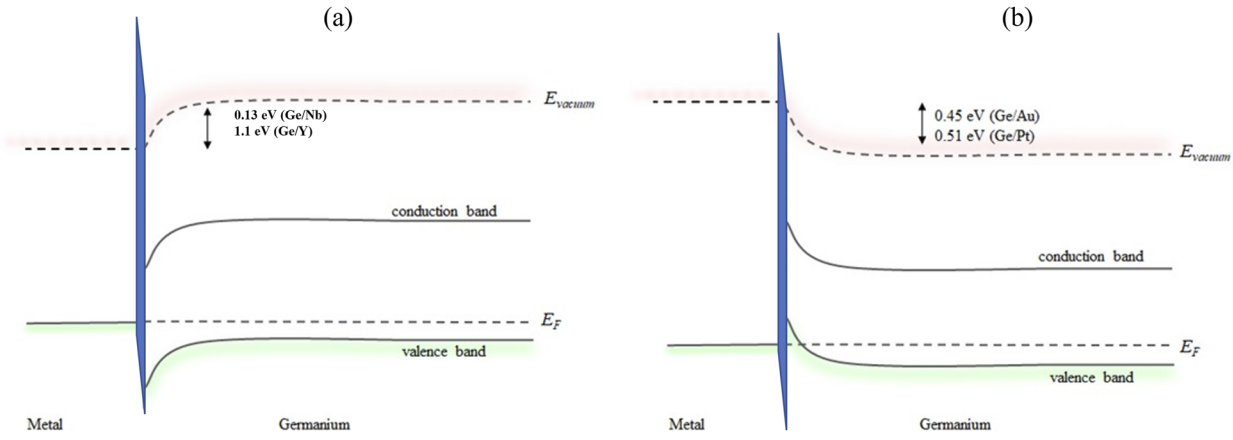

FIG. 6. Schematic of energy band alignment of the heterojunctions. (a) Y/Ge and Nb/Ge interface. (b) Au/Ge and Pt/Ge interface. Figure not to scale.

oxide. The bulk sensitive nature of HAXPES probes the buried semiconductor, and therefore, photoelectrons from the semiconductor pass through the interface region to be detected, while the photoelectrons from metal do not. The resulting shift in the binding energy of the semiconductor is, therefore, proportional to the interface dipoles and is reflected in the core-level binding energy difference $\Delta E_{CL} = (E_{Ge\ core\ line} - E_{CL})_{heterojunction}$. Thus, HAXPES offers the unique advantage of measuring the exact energy band alignment in heterojunctions even in the presence of a complex interface.

We can now calculate the valence band offset ΔE_V using the difference in the peak position of the metal and semiconductor for all interfaces studied. Although HAXPES measures ΔE_V, it is important to realize that for a metal–semiconductor interface, the Schottky barrier height gives the position of the metal Fermi level relative to the valence band maximum of the semiconductor (for P type semiconductors).[36] In other words, the magnitude of the measured valence band offset corresponds to the Schottky barrier height. The measured barrier heights, energy difference between the core levels for the different heterojunctions, and reference materials are listed in Table I, along with barrier heights predicted from Anderson's rule for comparison. As expected, Y on HPGe has a higher measured Schottky barrier height (1.10 ± 0.10 eV), confirming that it would be the better hole-blocking contact. The Schottky barrier calculated based on the work function difference is 1.57 eV. From Eq. (1), we can see that interface contribution will manifest as a core-level binding energy difference in the heterojunction, ΔE_{CL}. Although Nb is considered a potential hole-blocking contact due to the relatively low work function of the Nb(001) face (4.02 eV), the Schottky barrier (0.13 ± 0.10 eV) was lower than Y. This measurement demonstrates that Nb would not be as useful as a hole-blocking contact on Ge. Our measurement of Nb has similar deviation relative to the Anderson rule estimate as Y. For the electron-blocking contacts Au and Pt, we measured offsets of 0.45 ± 0.10 and 0.51 ± 0.10 eV, respectively. The vacuum levels of the Au and Pt are above that of Ge, thereby confirming that they would be ideal electron-blocking contacts. The energy band alignment of the heterojunctions is shown schematically in Fig. 6. We align the Fermi level across the interface and show the offset as difference in the vacuum level; the left-hand side of the figure shows the band alignment for the two low work function materials Y and Nb, while the right-hand side shows the energy band alignment of the high work function materials, Au and Pt.

IV. CONCLUSIONS

In summary, we have investigated the Schottky barrier heights for Y, Nb, Au, and Pt on HPGe with HAXPES. A high Schottky barrier is found for Y/HPGe, explaining its effectiveness as a hole-blocking contact. Conversely, a low barrier height is found for Nb/HPGe, showing that it would not be effective as a hole-blocking contact. We noticed a deviation in the barrier height from the classic Anderson rule. HAXPES revealed clear evidence of metal oxide formation in Y/Ge and Y/Nb interfaces. As expected, we see no evidence of metal oxide formation for Au/Ge and Pt/Ge interfaces. Clearly, work function alone does not give a complete picture of energy band alignment, and surface and interface chemistry also play a dominant role in energy band alignment.

ACKNOWLEDGMENTS

This research used resources of the National Synchrotron Light Source-II, which are U.S. DOE Office of Science Facilities, at Brookhaven National Laboratory under Contract No. DE-SC0012704. The research was partially funded by Grant No. DOE FWP PS016.

AUTHOR DECLARATIONS

Conflict of Interest

The authors have no conflicts to disclose.

Author Contributions

Abdul K. Rumaiz: Conceptualization (equal); Data curation (equal); Formal analysis (equal); Funding acquisition (equal); Investigation (equal); Project administration (equal); Writing – original draft

(equal); Writing – review & editing (equal). **Conan Weiland**: Data curation (equal); Formal analysis (equal); Methodology (equal); Writing – original draft (equal); Writing – review & editing (equal). **Ian Harding**: Formal analysis (supporting); Investigation (supporting); Writing – original draft (supporting); Writing – review & editing (equal). **Neha S. Nooman**: Data curation (equal); Formal analysis (equal); Methodology (equal); Visualization (equal). **Thomas Krings**: Investigation (supporting); Writing – original draft (supporting); Writing – review & editing (supporting). **Ethan L. Hull**: Conceptualization (supporting); Writing – original draft (supporting). **Gabriele Giacomini**: Formal analysis (supporting); Investigation (supporting); Writing – original draft (supporting); Writing – review & editing (supporting). **Wei Chen**: Formal analysis (supporting); Writing – original draft (supporting); Writing – review & editing (supporting). **Eric Cockayne**: Conceptualization (supporting); Formal analysis (equal); Investigation (equal); Software (lead); Writing – original draft (equal); Writing – review & editing (equal). **D. Peter Siddons**: Funding acquisition (equal); Project administration (equal); Supervision (equal); Writing – original draft (equal); Writing – review & editing (supporting). **Joseph C. Woicik**: Conceptualization (supporting); Data curation (supporting); Formal analysis (equal); Investigation (equal); Methodology (equal); Writing – original draft (equal); Writing – review & editing (equal).

DATA AVAILABILITY

The data that support the findings of this study are openly available in NIST repository at https://doi.org/10.18434/mds2-2623.[18]

REFERENCES

[1] W. A. Harrison, "Elementary theory of heterojunctions," in *Electronic Structure of Semiconductor Heterojunctions*, Perspectives in Condensed Matter Physics (A Critical Reprint Series) Vol. 1, edited by G. Margaritondo (Springer, 1988).

[2] F. Capasso, Science **235**, 172 (1987).

[3] S. Abbaszadeh, N. Allec, S. Ghanbarzadeh, U. Shafique, and K. S. Karim, IEEE Trans. Electron Devices **59**, 2403 (2012).

[4] P. A. Tove, Nucl. Instrum.Methods **133**, 445 (1976).

[5] X. Yang *et al.*, Joule **3**(5), 1314–1327 (2019).

[6] D. Protic and G. Riepe, IEEE Trans. Nucl. Sci. **32**, 553–555 (1985).

[7] H. L. Malm, IEEE Trans. Nucl. Sci. **22**, 140 (1975).

[8] D. Protic, T. Stohlker, T. Krings, I. Mohos, and U. Spillmann, IEEE Trans. Nucl. Sci. **52**, 3194–3198 (2005).

[9] A. K. Rumaiz *et al.*, IEEE Trans. Nucl. Sci. **61**, 3721–3726 (2014).

[10] E. Gatti and P. Rehak, Nucl. Instrum. Methods Phys. Res. **225**, 608 (1984).

[11] P. N. Luke, C. P. Cork, N. W. Madden, C. S. Rossington, and M. F. Wesela, IEEE Trans. Nucl. Sci. **39**, 590 (1992).

[12] E. L. Hull, R. H. Pehl, J. R. Lathrop, and B. E. Suttle, Nucl. Instrum. Methods Phys. Res., Sect. A **626–627**, 39 (2011).

[13] E. Hull, R. Pehl, B. Suttle, and J. Lathrop, U.S. patent US2011/0298.131 A1 (8 Dec 2011).

[14] G. Kresse and J. Furthmüller, Phys. Rev. B **54**, 11169 (1996).

[15] Certain commercial software is identified in this paper to adequately describe the methodology used. Such identification does not imply recommendation or endorsement by the National Institute of Standards and Technology, nor does it imply that the software identified is necessarily the best available for the purpose.

[16] J. P. Perdew, A. Ruzsinszky, J. Tao, V. N. Staroverov, G. E. Scuseria, and G. I. Csonka, J. Chem. Phys. **123**, 062201 (2005).

[17] E. Blöchl, Phys. Rev. B **50**, 17953 (1994); arXiv:1408.470.

[18] See https://doi.org/10.18434/mds2-2623 for NIST public data repository.

[19] C. Weiland, C. Jaye, N. F. Quackenbush, E. Gann, Z. Fu, J. P. Kirkland, B. A. Karlin, B. Ravel, J. C. Woicik, and D. A. Fischer, Synchrotron Radiat. News **31**, 23 (2018).

[20] R. L. Anderson, IBM J. Res. Dev. **4**, 283–287 (1960).

[21] J. Tersoff, Phys. Rev. B **30**, 4874(R) (1984).

[22] E. A. Kraut, R. W. Grant, J. R. Waldrop, and S. P. Kowalczyk, Phys. Rev. Lett. **44**, 1620 (1980).

[23] J. C. Woicik, E. J. Nelson, L. Kronik, M. Jain, J. R. Chelikowsky, D. Haskett, L. E. Berman, and G. S. Herman, Phys. Rev. Lett. **89**, 077401 (2002).

[24] A. K. Rumaiz, J. C. Woicik, E. Cockayne, H. Y. Lin, G. H. Jaffari, and S. I. Shah, Appl. Phys. Lett. **95**, 262111 (2009).

[25] A. Dimoulas, D. Tsoutsou, Y. Panayiotatos, A. Sotiropoulos, G. Mavrou, S. F. Galata, and E. Golias, Appl. Phys. Lett. **96**, 012902 (2010).

[26] R. Reichi and K. H. Gaukler, Appl. Surf. Sci. **26**, 196 (1986).

[27] D. Majumdar and D. Chatterjee, J. Appl. Phys. **70**, 988 (1991).

[28] Z. Q. Liu, W. K. Chim, S. Y. Chiam, J. S. Pan, S. R. Chun, Q. Liu, and C. M. Ng, Surf. Sci. **606**, 1638–1642 (2012).

[29] S. Doniach and M. Sunjic, J. Phys. C: Solid State Phys. **3**, 285 (1970).

[30] H. Tian *et al.*, Appl. Surf. Sci. **253**, 1236 (2006).

[31] N. Tabet, M. Faiz, N. M. Hamdan, and Z. Hussain, Surf. Sci. **523**, 68 (2003).

[32] S.-C. Lim, M.-C. Hsiao, M.-D. Lu, Y.-L. Tung, and H.-Y. Tuan, Nanoscale **10**, 16657 (2018).

[33] M. R. Alexander, G. E. Thompson, X. Zhou, G. Beamson, and N. Fairley, Surf. Interface Anal. **34**, 485 (2002).

[34] W. S. M. Werner, W. Smekal, and C. J. Powell, Simulation of Electron Spectra for Surface Analysis (SESSA) 2.2.0, National Institute of Standards and Technology, Gaithersburg, MD, 2021.

[35] S. M. Sze, *Physics of Semiconductor Devices* (Wiley, New York, 1969).

[36] *Heterojunction Band Discontinuities: Physics and Device Application*, edited by F. Capasso and G. Margaritondo (North-Holland, New York, 1987).

[37] H. B. Michaelson, J. Appl. Phys. **48**, 4729 (1977).